Tribology Letters, Vol. 23, No. 2, August 2006 (© 2006)
DOI: 10.1007/s11249-006-9059-y

The role of the cation in antiwear films formed from ZDDP on 52100 steel

Gavin Pereira[a], Andreas Lachenwitzer[a], David Munoz-Paniagua[a], Masoud Kasrai[a,*], Peter R. Norton[a], Mike Abrecht[b] and P.U.P.A. Gilbert[b,c]

[a]*Department of Chemistry, University of Western Ontario, London, Ontario N6A 5B7, Canada*
[b]*Synchrotron Radiation Center, University of Wisconsin—Madison, Stoughton, WI 53589, USA*
[c]*Physics Department, University of Wisconsin—Madison, Madison, WI 53706-I390, USA*

Received 20 January 2006; accepted 20 March 2006; published online 25 August 2006

Phosphorus L-edge and oxygen K-edge X-ray PhotoEmission Electron Microscopy (XPEEM) have been used to characterize the chemical nature of the cation present in tribochemical films via comparison with model Fe^{2+} and Zn^{2+} compounds. The results are contrasted to the P L-edge, P K-edge and S K-edge XANES data. The findings suggest that antiwear pads containing long chain zinc polyphosphate glass are formed at the points of asperity contact, and a thin, short chain zinc polyphosphate film is formed where no asperity contact is made. SEM/EDX measurements helped to elucidate the distribution of the elements, and strong spatial correlations were observed between P, O, Zn and S in the pads, indicating that they are composed mostly of zinc polyphosphates, especially near the surface. The zinc polyphosphate antiwear pads are characterized by a much lower modulus than that observed on the thin film regions, the latter being characteristic of the substrate steel.

KEY WORDS: ZDDPs, X-PEEM, cation, tribofilm, polyphosphate, nanoindentation

1. Introduction

Automotive components require a variety of lubricating oil additives and fluids to operate satisfactorily. The functionalities of the oils and fluids differ drastically depending on their intended usage and specific system requirements. One of the chemically active additives, zinc dialkyl dithiophosphate (ZDDP) has been used in internal combustion engines for at least 60 years, and is added to fully formulated oils as an antioxidant and antiwear additive. While other oil additives found in fully formulated oils may alter the functionality of ZDDPs, this molecule is known to interact with the metallic surface and form a protective film, which we call a tribochemical film, or tribofilm (also referred to as antiwear film).

A complex four-step mechanism scheme accounting for the decomposition of ZDDPs has been proposed by Willermet *et al.* [1]. Their film formation mechanism assumes adsorption on the metallic surface, followed by reaction of ZDDPs to form phosphates bound to the metal surface, followed by growth of the polyphosphate film, and termination by the metals ion available, typically zinc. Bancroft *et al.* [2] have proposed a different reaction pathway that depends on the availability of cations (Fe and/or zinc), and reaction temperature. Ferrari *et al.* [3] have proposed a two-step pathway involving the removal of the iron oxide layer by the reciprocating surface's rubbing motion, followed by reaction of ZDDPs with the nascent iron substrate.

Martin *et al.* [4] have applied Pearson's [5] hard and soft acids and bases (HSAB) principles to explain that phosphates (hard bases) preferentially react with harder acids. Since Fe^{3+} is a harder Lewis acid than Zn^{2+}, cation exchange is highly favored. This theory illustrates that with prolonged rubbing, and film growth, short chain polyphosphates are expected as the Zn^{2+} cations are exchanged with Fe^{3+} cations already present in the film, resulting in a faster termination of the phosphate network.

Excellent reviews on the history and evolution of ZDDPs [6], and a summary of the interaction of ZDDPs with metallic surfaces [7] can be found in literature.

Multi-element X-ray absorption near edge structure (XANES) analysis has been previously applied to ZDDP derived films [3,8–14], and shows that ZDDPs break down to form very thin (≤100 nm) chemically complex, sacrificial amorphous polyphosphate glass films at the point of contact between metallic surfaces in an engine.

Imaging X-ray absorption spectroscopy (XAS) techniques have greatly improved our capabilities to understand thin films and surfaces, over a wide range of sub-disciplines including archeology, materials science, physics, chemistry, anthropology, and marine studies to name a few [15–18]. Spatially resolved XANES data

*To whom correspondence should be addressed.
E-mail: mkasrai@uwo.ca

acquisition is achieved with a technique called X-ray photoelectron emission microscopy (XPEEM). This technique permits the acquisition of spatially resolved information (≤100 nm) on the chemistry of the absorbing species, which can be correlated with topography.

Canning *et al.* [19] were the first to employ XPEEM comparing the spectra obtained from large analysis areas to small analysis areas. Their results showed that unreacted ZDDP did not overlap with regions where polyphosphate had formed, and speculated that phosphate formed on regions that appeared to be asperities, while unreacted ZDDP remained unchanged in the valleys surrounding the asperity points.

Since this initial work, several other P L-edge XPEEM studies on steel and various Al–Si alloys have appeared [9,11,12,20–23], reporting correlations between the chemistry, the topography and mechanical response of the antiwear film. We report the use of multi-edge X-PEEM using both the oxygen K-edge and the phosphorus L-edge.

2. Experimental

2.1. Materials and preparation and composition of the substrate

The steel samples were manufactured from 52100 steel rods into circular disks at The University of Western Ontario with dimensions of 10 mm × 10 mm × 4 mm. The composition of 52100 steel is ~1% C, ~0.025% P, ~0.025% S, ~0.25% Si, ~0.25 –0.45% Mn, 1.3–1.6% Cr, and the balance as Fe. The disks were subsequently mechanically polished with a 6, 3, and finally 0.5 μm diamond pastes using turpentine solvent. They were washed with methanol in an ultrasonic bath and stored in air to dry.

2.2. Morphology and topography data acquisition

Atomic force microscope (AFM) topography images were recorded for all the samples in air, using a Nanoscope IIIa equipped with a Multimode™ head (Digital Instruments, Santa Barbara, CA). The images were collected in contact force mode with a V-shaped silicon nitride cantilever possessing a nominal spring constant of 0.12 N/m. The images were processed using Digital Instruments® software to determine the average surface roughness (R_a) and root mean squared (RMS) roughness R_{RMS}.

2.3. Antiwear film preparation

Antiwear films were made on the polished, 52100 steel disks in a Plint high frequency wear tester. The commercial ZDDP concentrate is a mixture of neutral and basic forms, consisting of secondary butyl (85%) and *n*-octyl (15%) groups. The 1.2% ZDDP solution (~0.1% P) was prepared using the desired weight of ZDDP and diluted using MCT-10 base oil supplied by Imperial Oil.

The 52100 steel coupons and cylindrical pins (11 mm × 6 mm diameter) were cleaned in an ultrasonic bath using a light hydrocarbon solvent, and then placed in the Plint high frequency wear tester. The 1.2% ZDDP solution was poured into the Plint wear tester and the steel pin was laid flat against the disk. A 220 N load was applied to the pin (resulting in ~135 MPa pressure after the experiment concluded), the temperature was raised to 100 °C and maintained throughout the experiment and the pin was reciprocated with a stroke length of 7 mm at a frequency of 25 Hz (0.35 m/s).

2.4. Chemical analysis

After each experiment, excess oil was removed from the disks using tissue paper and then the samples were rinsed in hexane. XANES data were obtained at the Canadian Synchrotron Radiation Facility (CSRF) [24], situated at the 1 GeV Aladdin storage ring, University of Wisconsin, Madison. Phosphorus and sulphur K-edge spectra were obtained on the double-crystal monochromator (DCM) [25] covering an energy range of 1500–4000 eV with photon resolution of 0.8 eV. Phosphorus and sulphur L-edge spectra were obtained on the Grasshopper soft X-ray beamline covering an energy range of 70–900 eV with photon resolution of 0.2 eV. The phosphorus and sulphur K- and L-edge spectra were calibrated using pure unreacted diisobutyl ZDDP. The analyzed area was about 2 mm × 2 mm. The photoabsorption spectra for both the model compounds and samples were recorded in the total electron yield (TEY) mode and fluorescence yield (FY) mode for both surface and bulk sensitivity [26]. All spectra shown in this paper are an average of two scans that were digitally combined and normalized, with a linear background subtracted using the BAN [27] program. The assignment of the fine structure in XANES was carried out using model compounds obtained by the authors or by comparison to previous results [9,10,28,29].

XPEEM data acquisition was performed using the Spectromicroscope for the PHotoelectron Imaging of Nanostructures with X-rays (SPHINX) [18,30] (ELMITEC GmbH) installed on the HERMON beamline using both the low energy grating (LEG) and the medium energy grating (MEG) at the 1 GeV Aladdin storage ring, University of Wisconsin, Madison. The sample is held at a high negative potential (−20 kV) and photoelectrons are accelerated and magnified through electron optics. The magnified photoelectrons are intensified by two microchannel plates and converted into a visible image by a phosphor screen. For details see refs. [18,30].

We acquire an image (~180 μm field of view) optimized to give ~0.2 eV resolution at the phosphorus L-edge (for details see refs. [18,20,30]). Image intensity

in XPEEM is proportional to the TEY and the surface sensitivity was limited by the escape depth of the secondary electrons at the phosphorus L-edge (3–5 nm) [31,32]. Spectromicroscopy images were taken with a 0.2 eV step size from high energy to low energy. A 100 μm field of view was chosen for the selected area with a resolution of ~200 nm per pixel. The images were combined to produce a three-dimensional data set or spectromicroscopy 'stack' [32] that was analyzed to extract detailed chemical information about the tribofilm using aXis2000 software [32–34]. The software allowed for selection of regions of several pixels in size to extract XANES spectra. Stacks were acquired at the phosphorus L-edge (130–144 eV) using the LEG on the beamline and the O K-edge (510–556 eV) using the MEG of the beamline and analyzed for differences in chemistry.

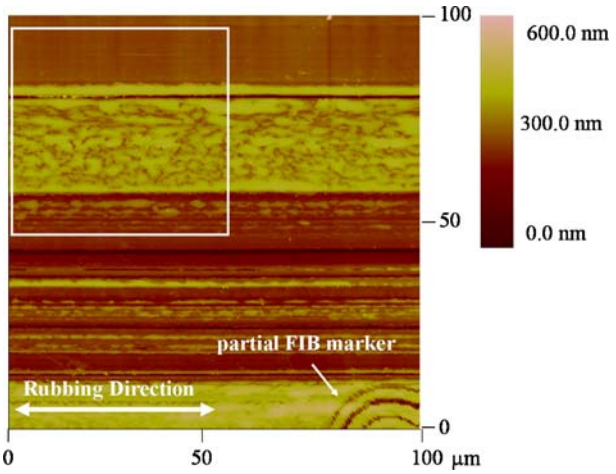

Figure 1. 100×100 μm^2 AFM height image of the region analyzed.

2.5. Mechanical analysis

The mechanical properties of the substrate and antiwear films were investigated using a Hysitron Triboindenter®, equipped with an optical microscope in which a desired area can be chosen in the field of view. This system has the capability to extract mechanical properties with very high force, spatial and depth resolutions. A Berkovich indenter with an elastic modulus (E_i) between 1000 and 1140 GPa, a Poisson ratio (v_i) of 0.07 and a tip radius of ~200 nm was used for all indentations. For experimental details see refs. [35–37], for a schematic see ref. [37].

Topographic images were obtained with ~2 μN force both prior to taking an indent and after indenting a region. The quasi-static measurements consisted of increasing the load to a chosen preset value via a constant velocity displacement of the indenter, followed by retraction at the same velocity. The loading process to the preset force, and unloading portion were all monitored. The elastic modulus was extracted using the Oliver–Pharr method [38] from the unloading section of the f–d curve. The films were investigated with a 50 μN maximum preset applied load.

3. Results and discussion

3.1. Antiwear film topography

Topographic images were taken on the antiwear film subsequent to the rubbing experiment. Figure 1 shows a general region of interest that was studied with multiple techniques. The rubbing direction is shown, which are parallel to the lines formed from contact with the reciprocating pin. Figure 1 shows half of one of the concentric markings made with Focused Ion Beam Milling (FIB) used for relocation of the same spot. The box in figure 1 is the region that was studied by multiple techniques and appears later as figure 8a.

The presence of elevated regions is evident (i.e., yellow area); these areas correspond to regions that carry the local load at or near the end of the wear experiment.

Figure 1 reveals a discontinuous film of varying thickness in all directions, consisting of patches (antiwear pads or tribofilm) elongated in the rubbing direction. This has been previously observed on steel surfaces [11,28,39,40].

3.2. XANES Chemical characterization

The sulphur K-edge XANES spectra collected in TEY mode are shown in figure 2, comparing unreacted ZDDP, Na_2SO_3, $ZnSO_4$, FeS, ZnS and the tribofilms spectra. The white line for ZDDP, peak 'b', is shifted with respect to the white lines of the other model compounds; to a higher photon energy compared to FeS (peak 'a'), or a lower photon energy, compared to ZnS (peak 'c'), SO_3^{2-} (peak 'd'), and SO_4^{2-} (peak 'e'). The shift is related to the oxidation state of the sulphur atom, and the local geometry of the absorbing atom [41,42]. For example, the oxidation state of sulphur in all the compounds FeS, ZDDP, and ZnS, is −2, but distinguishable shifts are noticed in the S K-edge XANES spectroscopy, which originate from the differences in the coordination of S to the other atoms in their respective compounds. This sensitivity is advantageous in the identification of the sulphur species present in the S K-edge XANES of the tribofilms.

The oxidized form of S is shifted to higher photon energy, as is evident in the spectra of Na_2SO_3, and $ZnSO_4$. The spectra collected on the tribofilm indicate the sulphur is present largely as ZnS, which has been previously observed from studies of ZDDPs forming tribofilms on steel surfaces [11,14]. The spectra of the tribofilm in figure 2 have been fit for all peaks aligning with ZDDP, ZnS, SO_3^{2-}, and SO_4^{2-} following a procedure reported in ref. [9]. A constant width for each peak was maintained during the fitting procedure. The

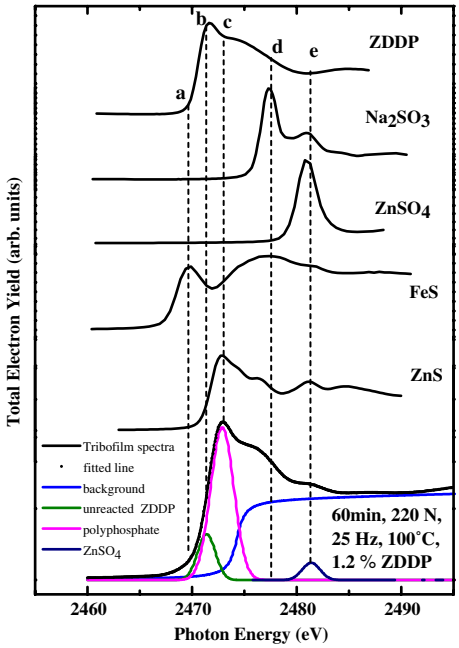

Figure 2. S K-edge XANES spectra collected in TEY mode of ZDDP, Na_2SO_3, $ZnSO_4$, FeS, and ZnS model compounds, and the tribofilm formed on steel under the conditions specified.

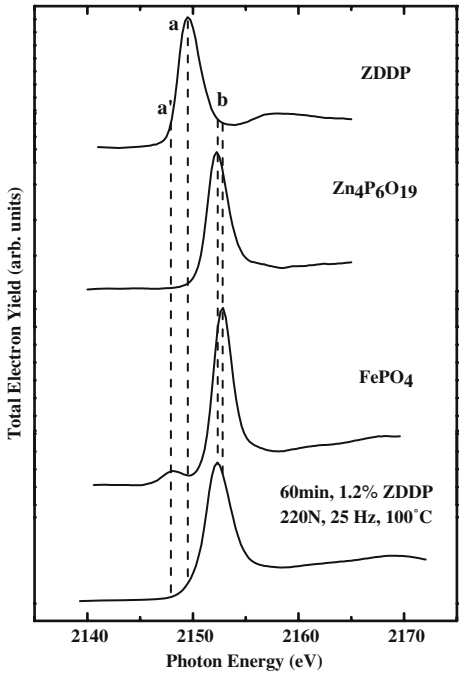

Figure 3. P K-edge XANES spectra collected in TEY mode of ZDDP, $Zn_4P_6O_{19}$, $FePO_4$ model compounds, and the tribofilm formed on steel under the conditions specified.

results of the de-convolution are shown in table 1. The alignment of ZDDP peak 'b' with the component of the fitted spectrum of the tribofilm indicates that unreacted ZDDP is present in the tribofilm. No FeS was found in the tribofilm, as expected since peak 'a' does not align with any noticeable features. The main sulphur-containing components of the tribofilm were found to be ZnS (~67%), and unreacted ZDDP (~12%). No evidence of SO_3^{2-} was found, otherwise peak 'd' would be much more intense. Any features aligned with peak 'd' are attributed to ZnS post-edge features.

The P K-edge XANES spectra of the tribofilm collected in TEY mode are shown in figure 3. The tribofilm spectra are compared to the spectra of ZDDP, $Zn_4P_6O_{19}$ and $FePO_4$. A single intense peak characteristic of the P K-edge is observed, which is attributed to the excitation of a phosphorus 1s electron to an empty p-like anti-bonding state [9,28,29]. The main peak of ZDDP (peak 'a') located at ~2149 eV is shifted with respect to the main peak of $Zn_4P_6O_{19}$ and $FePO_4$ (peak 'b'). The difference of ~2.5 eV agrees with previous results [9,28].

Table 1.
De-convoluted peak area percentage of the tribofilm from the sulphur K-edge spectra.

S K-edge			
FeS (%) 2469.9 eV	Unreacted ZDDP (%) 24741.8 eV	ZnS (%) 2472.9 eV	SO_4^{2-} (%) 2480.8 eV
0	~12	~75	~13

See text for further discussion.

The P K-edge XANES spectrum for the tribofilm clearly shows that after the experiment a phosphate has formed. Any spectral intensity that aligns with peak 'a' indicates that ZDDP is present in the phosphate film as an unreacted species. The area of the P K-edge XANES spectra for the tribofilm has been deconvoluted and fit for unreacted ZDDP and polyphosphate, as in our previous studies [9,22]. The results are summarized in table 2. The deconvolution indicated that ~11% of the P originated from unreacted ZDDP, which is consistent with the S K-edge XANES data and fitting. The remaining 89% of the P is present as a phosphate which L-edge data show is a polyphosphate glass (see below).

It is believed that the counter ion in the phosphate film is dependent on the available source(s) of cations. It

Table 2.
De-convoluted peak area percentage from peak fitting of the tribofilm for the phosphorus K- and L-edge XANES spectrum, and L-edge X-PEEM spectra.

P K-edge XANES		P L-edge XANES	
Unreacted ZDDP (%) 2149.4 eV	Polyphosphate glass formed (%) ~2152.0	Ratio of peaks a:c	Ratio of peaks b:c
~11	~89	0.36 0.52* 0.34**	0.29 0.46* 0.25**

'*' refers to spectra obtained in figure 5 from yellow regions (long chain polyphosphates).'**' refers to spectra obtained from blue regions (short chain polyphosphates).

has been speculated [29] that zinc is the primary cation, but the data in figure 3 show that there is too small a photon energy shift between the zinc phosphate model compound and the iron phosphate model compound to distinguish with certainty that zinc is the only cation present. However, absence of the weak shoulder labeled peak 'a'' in the spectrum of $FePO_4$ in the spectrum of the antiwear film, suggests that the phosphate counter ion is most likely a zinc (see XPEEM section).

The phosphorus L-edge XANES spectrum for the tribofilm collected in TEY mode is shown in figure 4, together with spectra for the model compounds, $Zn_4P_6O_{19}$, $FePO_4$, and ZDDP. The P L-edge XANES provides more information than the P K-edge, due to the narrower P L-edge linewidth and better photon resolution [28,29] and its greater sensitivity to the chemistry of the P-atom. The peak assignments have been discussed in detail in ref. [29]. The photon energy shift of the model compounds shows a similar behavior to the phosphorus K-edge spectra of the model compounds. Over the course of the experiment, peaks '1', '2' and '3' of ZDDP are shifted to peaks 'a', 'b', and 'c' of the tribofilm due to the change in chemistry of the ZDDP molecule to form a polyphosphate. Peak 'd' has been identified as a shape resonance peak, and is present when the absorbing atom (P) is coordinated to three or more electronegative atoms, such as oxygen, and is always present at the same energy position for all phosphates, whether crystalline or glassy [29]. The pre-edge shoulder of the tribofilm that aligns with peak '2' of ZDDP indicates presence of undecomposed ZDDP, which is consistent with earlier P and S K-edge XANES findings [9,29]. Peaks '4' and '5' develop from a second order C K-edge radiation at 285 eV, originating from beamline and sample contamination [20]. The spectra for the model compounds are taken on carbon tape, in which the second order contamination of carbon is intensified, whereas those peaks are weaker in the spectrum of the tribofilm. The spectra originate from a large area ($\sim$4 mm^2), thus represent an average over the area analyzed.

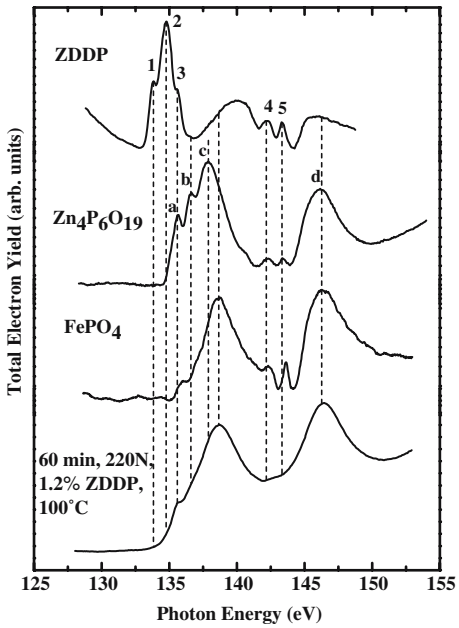

Figure 4. P L-edge XANES spectra collected in TEY mode of ZDDP, $Zn_4P_6O_{19}$, $FePO_4$ model compounds, and the tribofilm formed on steel under the conditions specified.

Yin *et al.* [43] have shown that the ratio of the fitted and deconvoluted peaks increase with increasing lengths of polyphosphates glasses. Deconvolution and fitting of the peaks present generates a reliable estimate of the species present. Their findings show that the ratio of a:c and b:c increase with increasing chain length of the polyphosphate glass and we have successfully used the technique in assessing the chain length of tribofilms [9,11,14,20,22,29]. The peak ratio of 'a' and 'b' relative to peak 'c' for our present tribolfilm is given in table 2, fit in the same manner as described previously [9,20]. An a/c ratio of approximately 0.44 or less (a:c $\leq \sim$0.44), corresponds to a short chain polyphosphate (less than 10 P atoms in a chain or network) [9]. An a/c ratio of approximately 0.60 or greater (a:c $\geq \sim$0.60) corresponds to long chain polyphosphates (greater than 25 P atoms in a chain/network). Ratios of a/c in between $\sim 0.44 < x < \sim 0.60$ represent medium chain polyphosphate chains or networks with P atoms ranging between 10 and 25. The findings listed in table 2 suggest borderline short-medium chain polyphosphates, which are consistent with previous finding generated on steel under similar conditions [7,14,20]. Nicholls *et al.* [28] and Zhang *et al.* [14] compared the spectra of the tribofilm versus iron ($FePO_4$) and zinc ($Zn_4P_6O_{19}$) phosphates using P L-edge XANES spectroscopy. For the tribofilm, both studies indicate similarities to the spectra of iron phosphate and zinc phosphate.

3.3. XPEEM chemical characterization

Details of the XPEEM microscope and data treatment are given elsewhere [11,17,18,21,23,30,44,45]. Unfortunately, the LEG provides photons at $\leq$ 144 eV, so our data are limited to a lower energy window, but useful chemical information can still be extracted from the spectra.

Figure 5a compares the background subtracted spectra used to obtain the distribution map, to spectra of ZDDP, $Zn_4P_6O_{19}$, and $FePO_4$. The contrasting internal spectra were obtained from regions of similar sized areas ($\sim$2 μm^2) on the SEM image through the P L-edge 'stack' the XPEEM microscope generates. The internal spectra are then matched to pixels or regions throughout the image, in which the software generates component maps. The P L-edge spectra obtained from the XPEEM were deconvoluted in the same manner as the P L-edge XANES spectra (see table 2), which show

presence of medium to long-chain polyphosphates (further referred to as long chain polyphosphates) and short chain polyphosphates. It has been previously shown that area averaged XANES using the fluorescence yield to measure absorption, provides a better measure of the bulk signal, compared to X-PEEM, which analyzes a smaller area, and has a smaller depth of analysis [9,21,30]. This could result in detection of different chemical species at the smaller length and depth scales.

The boxed region in figure 5b shows the SEM image obtained with the X-PEEM microscope that shows the region analyzed, which can be easily compared to figures 1, 5c and 6b.

A distribution map (figure 5c) was generated of the long chain polyphosphates (yellow regions) and short chain polyphosphates (blue region). Mixtures of long or short chain appear as dull areas. Regions that appear black are regions where the fit of the spectra is poor.

Mosey *et al.* [46] proposed a model that explains the formation of long chain polyphosphates through pressure induced cross-linking via zinc atoms in zinc phosphate. Nicholls *et al.* [20] were the first to observe experimental evidence for the theory, as their work on steel concluded that the highest pressures experienced at the surface of the large pads (load bearing surface) are responsible for the creation of the longest chain lengths and possible cross-linking of the chains. Our data are consistent with this picture as the longest chain length polyphosphates are found in the antiwear pads.

An O K-edge spectrum of the tribofilm obtained from the XPEEM microscope is shown in figure 6a, compared to the O K-edge XANES spectra of model compounds FeO, Fe_2O_3, $FePO_4$, the 52100 substrate, ZnO, and $Zn_3(PO_4)_2$. This edge is useful in assessing the role of Fe and Zn in the antiwear film on steel surfaces. The Fe compounds show spectral characteristics (pre-edge peaks 'a' and 'a') that are absent in the spectra of Zn compounds. De Groot *et al.* [47] have attributed the pre-edge split peaks to transitions from the O 1s to 2p states that are hybridized with the partially filled Fe 3d band that are separated by the ligand-field splitting. The pre-edge peaks in the spectra are absent for the Zn model compounds because of the filled 3d orbital. Peaks

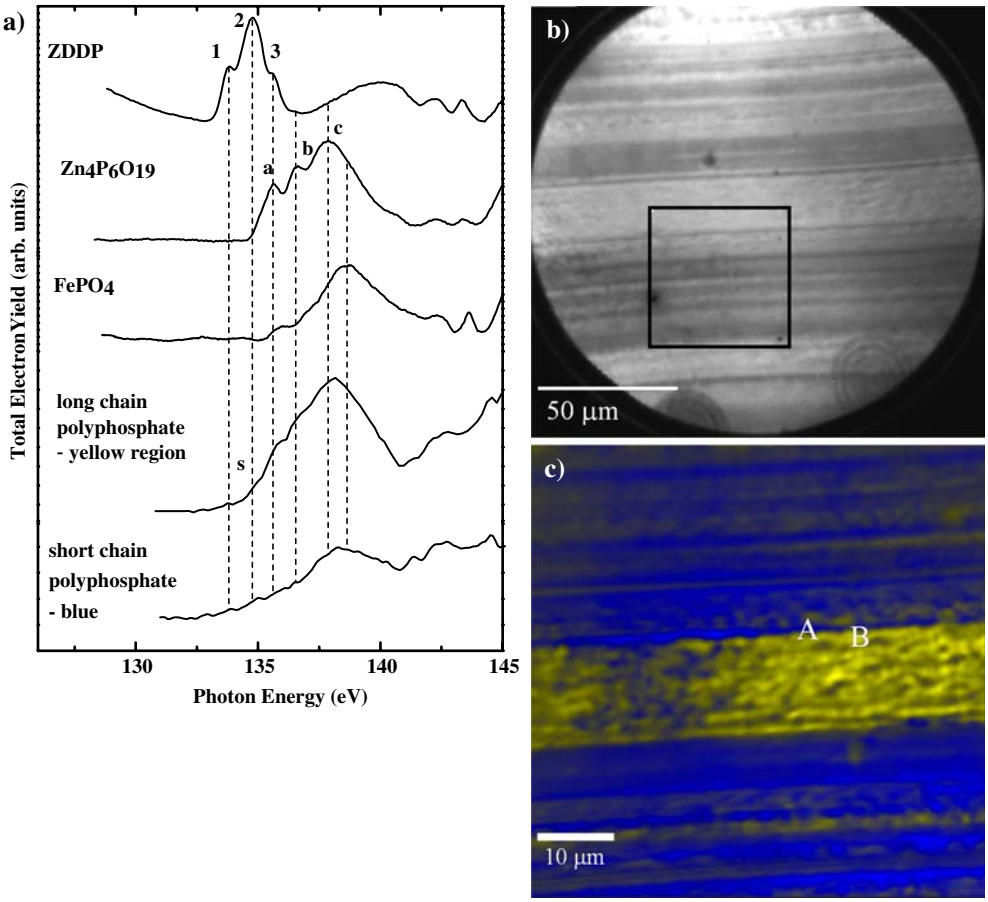

Figure 5. Phosphorus L-edge X-PEEM (a) Spectra of model compounds and spectra representative of long and short chain polyphosphates and (b) 50 μm radius SEM image obtained with the X-PEEM (c) distribution map of tribofilm. The yellow regions indicated long chain polyphosphate, and the blue areas represent areas of a weak phosphorus short chained species signal. Black areas are regions where the spectra were not fitted well with neither long nor short chain polyphosphate spectra. Regions of interest are indicated (labeled 'A' and 'B') and can be compared to other figures.

labeled 'b' and 'c' are attributed to the O 1s to O 2p transition that are hybridized with either the 4s or 4p of Fe or Zn [47–49]. The polished steel substrate shows an iron oxide consistent with Zhang *et al*. [14] investigation of the O K-edge of antiwear films. The spectral differences between $FePO_4$ and $Zn_3(PO_4)_2$ enable a differentiation between the phosphate formed at the surface based on the oxygen species detected. XANES of films derived from ZDDP show Zn^{2+} as the primary cation [14], but Auger depth analysis [50,51] and XPS depth profiling [14] has shown Fe as dominant in the bulk of the films.

The O K-edge spectra obtained clearly indicates two different types of oxygen are present in the region analyzed by XPEEM. A distribution map (figure 6b) was generated in the same manner as the P L-edge of the same area. We attribute the region color coded as red to zinc phosphate; this distribution is highly associated with the long chain polyphosphate (figure 5c). This information illustrates that the zinc is the principal cation present in the near surface region of the antiwear film and not iron, which agrees with the S K-edge XANES since no FeS was found. The region that is essentially iron oxide, which is colored coded as cyan, is strongly correlated to the short chain polyphosphate spectra from figure 5c. We know the iron oxide (cyan region) arises from the surface of the steel substrate and the AFM data suggest that the cyan regions were scarcely in contact with the reciprocating surface at the end of the wear experiment as this area looks almost pristine. We speculate that the short chain polyphosphate could either arise from the decomposition of ZDDP through a thermal process [52], by transfer from the partially formed antiwear pads, or as a result of a low load rubbed area.

Zhang *et al*. [14] found that the formation of ZnS is thermodynamically favored over the formation of FeS, and concluded that if any FeS does form, (not detected in our experiments; figure 2 peak 'a'), it is converted to ZnS. The authors [14] also applied the usage of Pearson's hard and soft acid and bases theory (HSAB) [5] first employed by Martin *et al*. [4] to investigate antiwear film formation. The soft base S^{2-} prefers to interact with the borderline soft acid Zn^{2+} over the harder Fe^{2+} or Fe^{3+}, which accounts for the formation of ZnS over FeS. But phosphates are hard bases, which should first react to form iron phosphates. Martin *et al*. [4] have suggested that zinc phosphate digests iron oxide, resulting in an exchange of Fe^{3+} cations with Zn^{2+} cations, causing the chain length to decrease with rubbing. Our findings are consistent with this picture, as the a:c ratio averaged from the TEY P L-edge XANES suggests a shorter chain polyphosphate in the bulk as compared to the near surface region (XPEEM; TEY). However, since the O K-edge spectrum for FeO and $FePO_4$ are similar, its not possible to distinguish between FeO + $Zn_3(PO_4)_2$ and Zn/Fe phosphate.

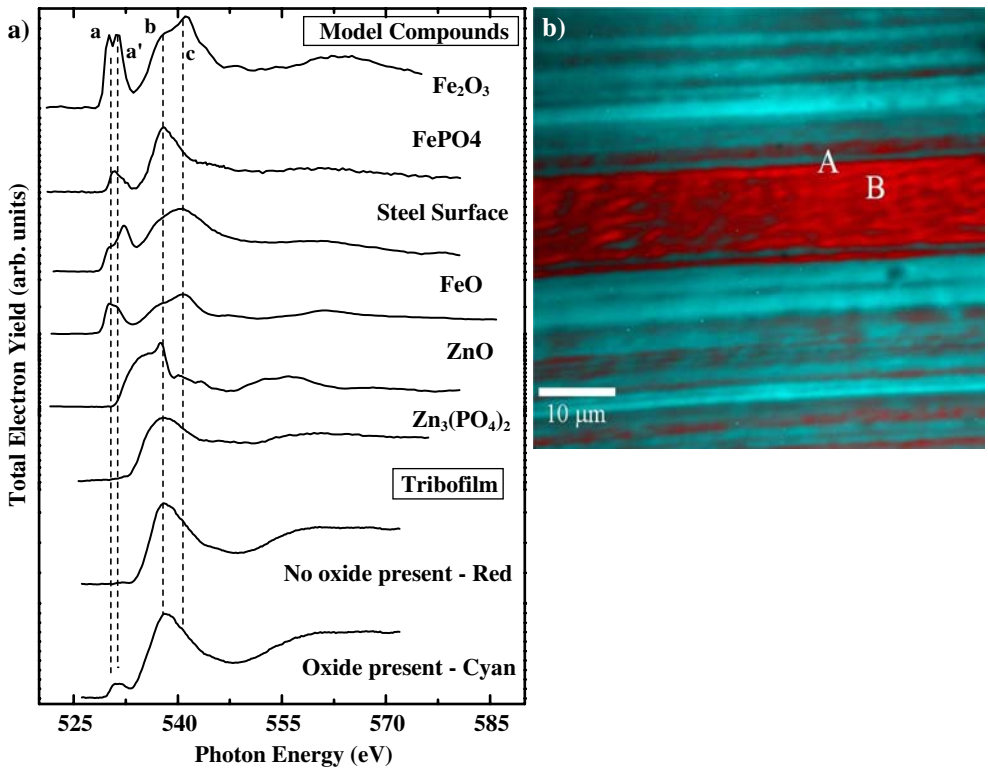

Figure 6. Oxygen K-edge X-PEEM (a) Spectra of model compounds and X-PEEM spectra extracted from the tribofilm and (b) distribution map of tribofilm. The cyan region indicates the presence of iron oxide; the red region indicates no iron oxide or iron phosphate. Black areas are regions where the spectra were not fitted well. Regions of interest are indicated (labeled 'A' and 'B') and can be compared to other figures.

An attempt was made to thin an antiwear film section using a focused ion beam (FIB) to the near interface region, but we found the influence of the steel substrate in the spectra (resulting from the removal of the film) masked the O K-edge data and thus we could not obtain conclusive evidence of zinc phosphate, iron phosphate or a mixture near the interface.

3.4. EDX/SEM chemical and morphological characterization of substrate

Mapping EDX/SEM of the region analyzed by XPEEM was employed to characterize the elemental distribution of the antiwear film and of the surface of the substrate. Figure 7a shows a field emission SEM image obtained at 5.0 kV beam energy to enhance surface sensitivity. Figures 7b–f are EDX elemental maps for Fe, O, P, S, and Zn, respectively. The brighter regions correspond to an increased abundance of the respective element. An EDX map was generated for carbon, but not shown since carbon was found to be sparsely distributed everywhere. Previous studies show that XPEEM is truly a surface sensitive technique sampling ~2–5 nm into the material [21,23,30,52], while EDX samples depths on the micron scale, and is employed as a bulk sampling technique compared to XPEEM. There is a very good correlation between the EDX maps, the AFM topography and the distribution maps generated from X-PEEM.

The EDX analysis confirms that regions containing long chain polyphosphates (figures 5 and 6), are rich in P, S, Zn and O. Fe is detected in this region, but at reduced concentrations, and could arise from the substrate. Comparing figures 5 and 6 to figure 7, we also confirm a correlation between the locations of the short chain polyphosphates and iron oxide, again suggesting that the Fe and O signals arise from the steel substrate.

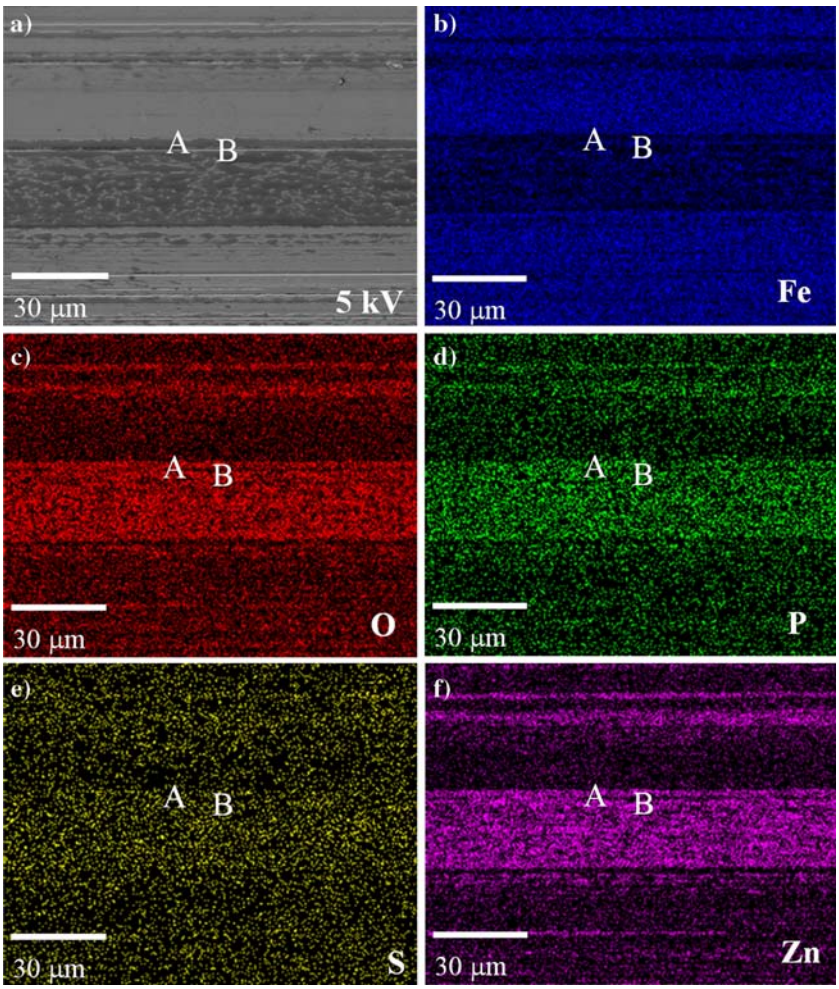

Figure 7. (a) Field emission SEM image and (b) mapping EDX of the region analyzed by the X-PEEM. Brighter areas in the EDX map indicate an abundance of that particular element (shown in the bottom right corner of the image). Both the SEM image and EDX maps were acquired at 5.0 kV, and 17 mm working distance. Regions of interest are indicated (labeled 'A' and 'B') and can be compared to other figures.

3.5. Mechanical evaluation

Nanoindentation measurements were performed at room temperature on the region studied by AFM, X-PEEM and EDX/SEM. Topography images were taken first on the regions with the same tip used to carry out the indentation. The maximum indentation load used to analyze the tribofilm was 50 μN applied in open-loop mode with a constant loading rate of 10 μN/s and then held for 5s and unloading with a constant rate of 10 μN/s. Indentation curves are analyzed using the Oliver and Pharr [38,53,54] method, in which the top 30% of the slope of the of the unloading curve (S) can be equated to the reduced modulus (E_r) and projected contact area (A) of the sample through equation (1) [38]:

$$S = \frac{dP}{dh} = \frac{2}{\sqrt{\pi}} E_r \sqrt{A}. \quad (1)$$

The reduced modulus (E_r) can be related to the elastic modulus (E_s) of the sample as shown in equation 2, if the Poisson ratio (v_i) and elastic modulus (E_i) of the indenter are known, and the Poisson ratio of the sample is also known.

$$\frac{1}{E_r} = \frac{(1-v_s^2)}{E_s} + \frac{(1-v_i^2)}{E_i}. \quad (2)$$

The three-sided diamond Berkovich indenter has very well defined properties, the elastic modulus is between 1000 and 1140 GPa, and possesses a Poisson's ratio of 0.07, while the tip radius is approximately ~200 nm. The generally accepted value of the Poisson ratio for 52100 steel is ~0.277 [55], but the Poisson ratio for the antiwear films remains immeasurable. Therefore, we report the indentation modulus (E_s^*) shown in equation 3, which corrects for tip compliance and is independent of the Poisson ratio of the film.

$$E_s* = \frac{E_s}{(1-v_s^2)} = \left[\frac{1}{E^*} - \frac{(1-v_i^2)}{E_i}\right]^{-1}. \quad (3)$$

Our analysis found two mechanically distinct regions of the antiwear film. Figure 8a shows an AFM image of the box-region illustrated in figure 1. Arrows point to the various locations studied by nanoindentation. Figure 8b shows two curves representative of the areas analyzed. The blue curve yields an E_s^* of 289 ± 16 GPa, indicative of the 52100 steel substrate [56] or iron oxide (results not published), while the red curve has a more plastic profile, and an E_s^* of 82 ± 18 GPa. The red curve was taken on regions where the antiwear zinc phosphate film has formed (figure 6b), and the blue curve is extracted from a cyan region. The antiwear film was found dispersed on the steel substrate, and the indentation modulus was comparable to the Interfacial Force Microscope (IFM) analysis on small alkyl-ZDDP derived pads which was ~74 ± 20 GPa [39], and previous studies of the response of antiwear films on 52100 steel [9,11,12,20,28,56]. Figure 8a also shows the values of the modulus determined for a number of locations and the data demonstrate clearly that the areas associated with the lower moduli coincide with the presence of antiwear pads. The data are consistent with previous studies [6,7] and indicate that the pads are associated with zinc polyphosphates, and that the modulus of the pads is much lower than steel and that they act to prevent the rubbing of steel-on-steel.

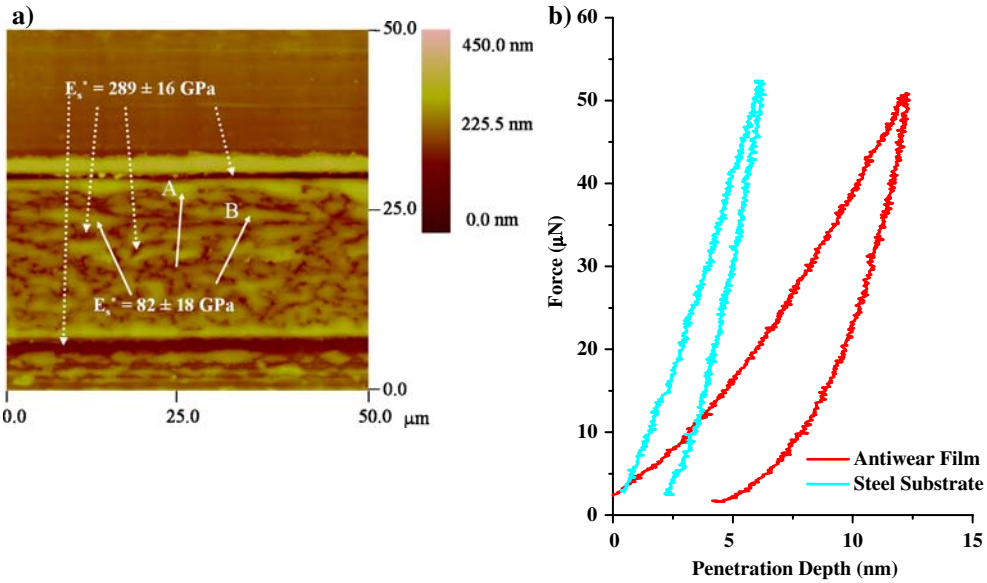

Figure 8. (a) The 50×50 μm^2 AFM area examined by X-PEEM, SEM, and mapping EDX. The indentation moduli for different regions are explained in detail in the text. (b) 50 μN force–distance (f–d) curves taken on the antiwear film. Imaging indentation permits selectivity of a feature to within ~60 nm resolution. Evidence is found that the cyan region differs mechanically from the antiwear wear film (red curve). See text for details.

4. Summary and conclusions

Analysis of the S-K edge, P L-edge and O K-edge XANES of ZDDP derived antiwear films has been undertaken. Used in conjunction with complementary scanning probe methods (AFM, SEM/EDX and imaging nanoindentation), the XANES data have yielded useful new information on the chemistry of these important materials as related to their function in automotive lubrication.

In summary;

(1) The specific area analyzed with the AFM showed two distinct regions, the lower region confirmed mechanically to be 52100 steel, and the other a mechanically softer, patchy and discontinuous film.
(2) The S K-edge XANES provided evidence for unreacted ZDDP and ZnS. The presence of SO_4^{2-}, and SO_3^{2-}, could not be definitively proved or disproved.
(3) The P XANES showed on average the presence of short to medium chain polyphosphates, while the P L-edge XPEEM spectra showed areas with long and short chain polyphosphates corresponding to the different regions of the film shown in the AFM data.
(4) The O K-edge XPEEM spectra enabled us to state that the surface of the antiwear film is exclusively a zinc based phosphate and not an iron phosphate. The region, where the pre-edge peak appears, is believed to be caused either by a bare steel substrate or one covered by an extremely thin, short chain polyphosphate film.
(5) SEM/EDX enabled us to confirm the presence of Fe in regions where the steel substrate is exposed and a weak iron signal where the phosphate glass is present; however the EDX maps for Zn, P and S and O are highly correlated.

Acknowledgments

The authors would like to thank Mr. Phil Shaw and Mr. Brian Dalrymple of the Physics Machine Shop and Dr. Leighton Coatsworth (all from The University of Western Ontario) for useful discussions. We acknowledge Dr. Brian Hart, Mr. Ross Davidson and Mr. Mark Biesinger all from Surface Science Western (SSW) located at The University of Western Ontario for help in acquiring XPS (not shown) and mapping EDX/SEM data. We are also grateful to Dr. Astrid Jürgensen and Dr. Franziskus Heigl from the Canadian Synchrotron Radiation Facility (CSRF), University of Wisconsin, Madison, for their technical support, and the National Science Foundation (NSF) for supporting the SRC under grant # DMR-0537588. This work was financially supported by the Natural Sciences and Engineering Research Council of Canada (NSERC), General Motors of Canada Ltd., General Motors R&D center and by the National Research Council of Canada (NRC) which supports the Canadian Synchrotron Radiation Facility at the Aladdin ring in Stoughton, Wisconsin.

References

[1] P.A. Willermet, D.P. Dailey, R.O. Carter III, P.J. Schmitz and W. Zhu, Tribol. Intl. 28 (1995) 177.
[2] G.M. Bancroft, M. Kasrai, M. Fuller, Z. Yin, K. Fyfe and K.H. Tan, Tribol. Letts 3 (1997) 47.
[3] E.S. Ferrari, K.J. Roberts, M. Sansone and D. Adams, Wear 236 (1999) 259.
[4] J.M. Martin, Tribol. Letts 6 (1999) 1.
[5] R. Pearson, J. Amer. Chem. Soc. 85 (1963) 3533.
[6] H. Spikes, Tribol. Letts 17 (2004) 469.
[7] M.A. Nicholls, T. Do, P.R. Norton, M. Kasrai and G.M. Bancroft, Tribol. Intl 38 (2005) 15.
[8] Z. Zhang, M. Kasrai, G.M. Bancroft and E. Yamaguchi, Tribol. Letts 15 (2003) 377.
[9] G. Pereira, A. Lachenwitzer, M.A. Nicholls, M. Kasrai, P.R. Norton and G. De Stasio, Tribol. Letts 18 (2005) 411.
[10] Z. Yin, M. Kasrai, M. Fuller, G.M. Bancroft, K. Fyfe and K.H. Tan, Wear 202 (1997) 172.
[11] M.A. Nicholls, G.M. Bancroft, P.R. Norton, M. Kasrai, G. De Stasio, B.H. Frazer and L.M. Wiese, Tribol. Letts 17 (2004) 245.
[12] M.A. Nicholls, G.M. Bancroft, P.R. Norton, M. Kasrai, G. De Stasio and L.M. Wiese, Tribol. Letts 18 (2004) 261.
[13] Z. Yin, M. Kasrai, M. Fuller, G.M. Bancroft, K. Fyfe, M.L. Colaianni and K.H. Tan, Wear 202 (1997) 192.
[14] Z. Zhang, E. Yamaguchi, M. Kasrai, G.M. Bancroft, X. Liu and M.E. Fleet, Tribol Letts 19 (2005) 221–229.
[15] G. Margaritondo and G. De Stasio, Intl J. Imag. Sys. Technol. 8 (1997) 188.
[16] G. De Stasio and G. Margaritondo, J. Electr. Spectr. Related Phenom. 84 (1997) 137.
[17] G. De Stasio, B.H. Frazer, B. Gilbert, K.L. Richter and J.W. Valley, Ultramicroscopy 98 (2003) 57.
[18] B.H. Frazer, M. Girasole, L.M. Wiese, T. Franz and G. De Stasio, Ultramicroscopy 99 (2004) 87.
[19] G.W. Canning, M.L. Fuller, G.M. Bancroft, M. Kasrai, J.N. Cutler, G. De Stasio and B. Gilbert, Tribol. Letts 6 (1999) 159.
[20] M.A. Nicholls, P.R. Norton, G.M. Bancroft, M. Kasrai, T. Do, B.H. Frazer and G. De Stasio, Tribol. Letts 17 (2003) 205.
[21] G. Pereira, A. Lachenwitzer, M. Kasrai, P.R. Norton, T.W. Capehart, T.A. Perry, Y.-T. Cheng, B. Frazer and G. De Stasio, Tribol. Letts (2006) in press.
[22] M.A. Nicholls, P.R. Norton, G.M. Bancroft and M. Kasrai, Wear 257 (2004) 311.
[23] M.A. Nicholls, G.M. Bancroft, M. Kasrai, P.R. Norton, B.H. Frazer and G. De Stasio, Tribol. Letts 18 (2005) 453.
[24] G.M. Bancroft, Can. Chem. News 44 (1992) 15.
[25] B.X. Yang, F.H. Middleton, B.G. Olsson, G.M. Bancroft, J.M. Chen, T.K. Sham, K. Tan and D.J. Wallace, Rev. Sci. Instr. 63 (1992) 1355–1358.
[26] M. Kasrai, Z. Yin, G.M. Bancroft and K. Tan, J. Vacuum Sci. Technol. A 11 (1993) 2694.
[27] T. Tyliszczak, McMaster University, unpublished program.
[28] M.A. Nicholls, T. Do, P.R. Norton, G.M. Bancroft, M. Kasrai, T.W. Capehart, Y.T. Cheng and T. Perry, Tribol. Letts 15 (2003) 241.
[29] M. Suominen-Fuller, M. Kasrai, G.M. Bancroft (2002) in: *Advanced Series in Physical Chemistry: Part 2*,Vol. 12B, ed. T.K. Sham (World Scientific Publishing Co., New Jersey, 2002).

[30] B. Frazer, B. Gilbert, B. Sonderegger and G. De Stasio, Surf. Sci. 537 (2003) 161.
[31] M. Kasrai, W.N. Lennard, R.W. Brunner, G.M. Bancroft, J.A. Bardwell and K.H. Tan, Appl. Surf. Sci. 99 (1996) 303.
[32] C. Jacobsen, S. Wirick, G. Flynn and C. Zimba, J. Microscopy 197 (2000) 173.
[33] L.M. Croll, J.F. Britten, C. Morin, A.P. Hitchcock and H.D.H. Stöver, J. Synchrotron Radiat. 10 (2003) 265.
[34] A. Hitchcock, P. Hitchcock, C. Jacobsen, C. Zimba, B. Loo, E. Rotenberg, J. Denlinger and R. Kneedler, aXis 2000—Analysis of X-ray Images and Spectra. http://unicorn.mcmaster.ca/aXis2000.html.
[35] A.C. Lund, A.M. Hodge and C.A. Schuh, Appl. Phys. Letts 85 (2004) 1362.
[36] C.A. Schuh, A.C. Lund and T.G. Nieh, Acta Mater. 52 (2004) 5879.
[37] C.A. Schuh, J.K. Mason and A.C. Lund, Nat. Mater 4 (2005) 617.
[38] W.C. Oliver and G.M. Pharr, J. Mater. Res. 7 (1992) 1564.
[39] O.L. Warren, J.F. Graham, P.R. Norton, J.E. Houston and T.A. Michalske, Tribol. Letts 4 (1998) 189.
[40] A. Tonck, J.M. Georges, R.C. Coy, J.C. Bell and G.W. Roper (1999) in: *Lubrication at the Frontier*, Vol. 36. ed. M. Priest (Elsevier, Amsterdam, 1999).
[41] M. Kasrai, J.R. Brown, G.M. Bancroft, Z. Yin and K.H. Tan, Intl J. Coal Geol. 32 (1996) 107.
[42] G.P. Huffman, S. Mitra, F.E. Huggins, N. Shah, S. Vaidya and F. Lu, Energy Fuels 5 (1991) 574.
[43] Z. Yin, M. Kasrai, G.M. Bancroft, K.H. Tan and X. Feng, Phys. Rev. B 51 (1995) 742.
[44] G. De Stasio, B. Gilbert, B.H. Frazer, K.H. Nealson, P.G. Conrad, V. Livi, M. Labrenz and J.F. Banfield, J. Electr. Spectr. Related Phenom. 114–116 (2001) 997.
[45] B. Frazer, B. Gilbert and G. De Stasio, Rev. Sci. Instr. 73 (2002) 1373.
[46] N.J. Mosey, M.H. Müser and T.K. Woo, Science 307 (2005) 1612.
[47] F.M. De Groot, M. Grioni, J.C. Fuggle, J. Ghijsen, G.A. Sawatzky and H. Petersen, Phys. Rev. B 40 (1989) 5715.
[48] M. Pollak, M. Gautier, N. Thromat, S. Gota, W.C. Mackrodt and V.R. Saunders, Nucl. Instr. Methods Phys. Res. B 97 (1995) 383.
[49] Z.Y. Wu, S. Gota, F. Jollet, M. Pollak, M. Gautier-Soyer and C.R. Natoli, Phys. Rev. B 55 (1997) 2570.
[50] J.M. Martin, C. Grossiord, T. Le Mogne, S. Bec and A. Tonck, Tribol. Intl 1 (2001) 523.
[51] Z. Zhang, E.S. Yamaguchi, M. Kasrai and G.M. Bancroft, Tribol. Trans. 47 (2004) 527.
[52] G. De Stasio, B. Gilbert, O. Fauchoux, M. Capozi, P. Perfetti, G. Margaritondo and B.P. Tonner, Rev. Sci. Instr. 70 (1999) 1740.
[53] G.M. Pharr and W.C. Oliver, MRS Bulletin 17 (1992) 28.
[54] W.C. Oliver and G.M. Pharr, J. Mater. Res. 19 (2004) 3.
[55] Y.B. Guo and C.R. Liu, J. Manuf. Sci. Eng. 124 (2002) 1.
[56] G. Pereira, D. Munoz-Paniagua, A. Lachenwitzer, M. Kasrai, P.R. Norton, T.W. Capehart, T.A. Perry and Y.-T. Cheng, Wear (2006) in press.